

Chapter 3

Numerical Simulation and Experimental Study on Internal Flow Characteristic in the Dynamic Fluidic Sprinkler



Abstract A detailed study of the relationship between velocity distribution, length of tube and nozzle sizes was conducted using a dynamic fluidic sprinkler. Therefore, the objectives of this chapter were to study (1) inner flow characteristics of dynamic fluidic sprinkler. (2) compare numerical simulation and experimental results (3) to introduce an empirical equation of the variation trend of rotation speed for the newly designed sprinkler. A mathematical model for simulation of the inner flow distribution of the sprinkler was obtained by using computational fluid dynamics. The results were validated by numerical simulation and compared to the experimental results. The results revealed that the nozzle diameter, length of the tube and the operating pressure had a significant influence on the rotation speed of the sprinkler. This study provides baseline information to improve water application efficiency for crop production in sprinkler irrigated fields.

Keywords Inner flow · Nozzle · numerical simulation · Water saving

3.1 Introduction

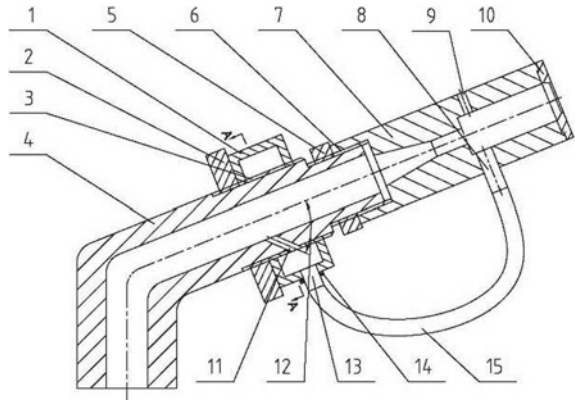
Water-use efficiency (WUE) in crop production is a major problem in the design and management of irrigation systems. Sprinkler irrigation is characterized by high-potential irrigation efficiency [1], and it has been widely used in agriculture for water conservation. The sprinkler head is regarded as a key component of any sprinkler irrigation system, and its hydraulic performance can affect the irrigation efficiency of sprinkler systems. Most studies about sprinkler irrigation have focused on hydraulic performance [2, 3]. An analysis of the flow behavior of the water flow in the sprinkler inner field is also important to understand the micro-characteristics of the sprinkler. Many investigators have applied CFD as a numerical simulation tool to carry out different investigations on sprinkler irrigation. Wang (2006) analyzed the flow characteristics in the emitter used in the drip irrigation inner field using computational fluid dynamics (CFD) techniques. Some basic studies have been performed on the inner flow characteristics of sprinklers. In 1933, the designer at the company Rainbird [4] developed an impact sprinkler for the first time. The inner flow characteristics

of the sprinkler compartment and pressure losses were analyzed using ANSYS software [5–7]. A 3D turbulent simulation was used to analyze the flow behavior and compared the flow rate, static pressure distribution and kinetic energy values of the sprinkler [8]. Their results indicated that the turbulence model can accurately predict the working pressure and the relationship between the outlet velocities.

In 2005, researchers at Jiangsu University in China developed a new type of fluidic sprinkler. Its principle of operation is based on the “Coanda effect” to perform the function of rotation. Several theoretical, numerical and experimental studies have been conducted to improve the structural and hydraulic performance of the complete fluidic sprinkle. Palfrey and Liburdy [9] studied the main flow characteristic of the turbulent offset jet. Bourque and Newman [10] studied the mean flow characteristic of the wall-attaching offset jet. Hoch and Jiji [11] also researched into a numerical prediction of the jet trajectory and jet reattachment length. Their researcher works revealed that when the primary flow jet becomes reattached to the right side, the pressure in the two sidewalls of the main jet flow exclusively depends on flowing duct length and operating pressure. Song et al. [12] studied the flow and heat transfer characteristics of the 2D jet. Their study demonstrated that the structural optimization approach can be effectively implemented by CFD simulation. Wang and Lu [13] studied the basic theory of wall attachment fluidic; their research was based on only 2D flow. Liu et al. [14] studied numerical and experimental studies on a new type of variable rate of the fluidic sprinkler. Zhu et al. [15] carried out the study on flow characteristics of a wall attaching offset jet in a complete fluidic sprinkler.

They concluded that the results obtained from the numerical simulation could reflect the inner flow of a complete fluidic sprinkler. Dwomoh et al. [16] compared fluidic and impact sprinklers and concluded that variations in quadrant completion times were small for both fluidic and impact sprinklers. Similarly, Hu et al. [17] carried out a study on the fluidic sprinkler and confirmed the need to optimize the structure. Based on their recommendations, a newly designed dynamic fluidic sprinkler was invented by the Research Centre of Fluid Machinery Engineering and Technology, Jiangsu University China. The sprinkler is comparatively cheaper, simple to construct, low consumption of energy and price. No previous studies investigated numerical simulation on dynamic fluidic sprinkler. Therefore, the objectives of this paper were to study (1) inner flow characteristics of the dynamic fluidic sprinkler (2) compare Numerical simulation and experimental results based on rotation speed time using CFD program FLUENT software. (3) introduce the empirical equation of the variation trend of rotation speed for the newly designed sprinkler.

Fig. 3.1 Schematic, pictorial view of the newly fluidic sprinkler head. 1. Water signal tank. 2. First, lock nut. 3. Pipe sprayer 4. Spray body. 5. Second lock nut. 6. Body of the fluidic element. 7. Jet element body. 8. Water inlet. 9. Airhole. 10. Outlet cover plate. 11. Water dividing hole. 12. α degree. 13. Signal nozzle. 14. Third lock nut. 15. Conduit



3.2 Materials and Methods

3.2.1 Design of Newly Dynamic Fluidic Sprinkler Type

Figure 3.1 presents the structure of a dynamic fluidic sprinkler. The profile of the fluidic element was defined by the inner contraction angles, the offset length, and the working area. A prototype of the dynamic fluidic sprinkler was self-designed and locally machined by using a wire-cut electric discharge machining process. The manufacturing tolerance for the size was within 0.02 mm as shown in Fig. 3.1. The working theory of dynamic fluidic sprinkler is based on the theory of the Coanda effect. Water flows from the diameter into the action zone, and the main jet is ejected from the central circular hole. The left and the right sides of the main jet are separated from each other, and the air at both ends is out of circulation. By opening the reverse air hole of left allows air to be pumped into the left cavity. The air gap between the exit at the right side of the element and the water jet is filled by air, such that the pressures on both sides of the main jet are basically equal. At the same time, the nozzle receives the signal water on the left edge of the water jet, then the signal water flows in the tube to the inlet signal [18–20].

3.2.2 Design of the Nozzles

Most sprinklers have two nozzles, the main nozzle and an auxiliary nozzle that discharge water in the form of a jet into the air. Nozzles with different diameters are the principal parameters that affect the hydraulic performances of sprinklers. Circular nozzles are commonly used on fluidic sprinklers due to the advantages of the large spray range and simple configurations and convenience to machine [21].

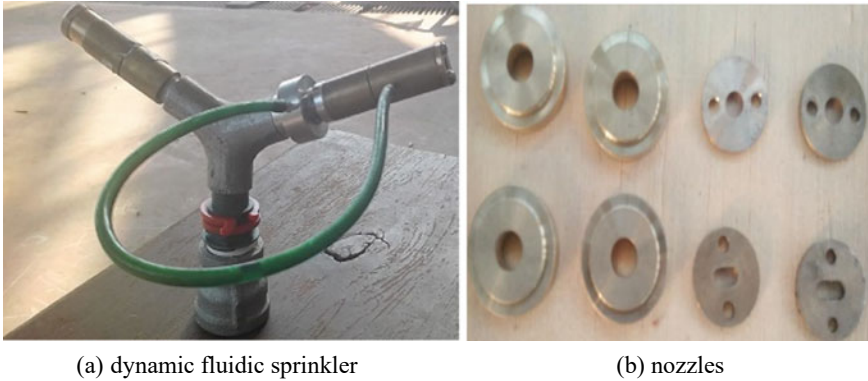


Fig. 3.2 A prototype of the dynamic fluidic sprinkler and nozzle sizes

Therefore, the test nozzles were self-designed and locally machined using a wire-cut electric discharge machining (EDM) process. The prototypes of the nozzles are shown in Fig. 3.2. The inlet diameter of the nozzle was set as 15 mm, while the outlet diameters were chosen as 3, 4, 5, 6, and 7 mm.

3.2.3 Numerical Simulation

Dynamic fluidic sprinkler which consists of a fluidic element and contraction angle was employed in this study. The three-dimensional model of the dynamic fluidic sprinkler is illustrated in Fig. 3.3. The commercial code ANSYS fluent 19.2 was adopted to conduct the numerical calculation. The full flow fields were divided into different fluid domains and each of them was meshed by unstructured hexahedron mesh via FLUENT CFD. This sprinkler works under variable pressure because of the pressure-adjusting device, that is, the inlet of the sprinkler does not keep a fixed pressure. As can be seen in Fig. 3.4, in the variable-rate fluidic sprinkler, one of the moving inserts is stationary and is referred to as the static insert. The pressure at the different rotating angles of the sprinkler was adjusted. The movement insert and static insert were in the rotating angle of 0 to 90 degrees and the black part was the flow cross-section. The movements insert rotated deasil and the angle increased as the sprinkler rotates. For square spraying shape, the varied flow cross-section from 0° to 90° is the same with 90° to 180°, from 180° to 270° is the same with 90° to 180°, from 0° to 180° is the same with 270° to 360°. In ANSYS fluent under the reference frame, the moving insert was set as frame and mesh motion, the rotational velocity $\omega = 0.07$ rad/s was obtained from a plot of the moment against angular velocity and under the relative to a cell, the zone was set as a rotor. Equation (3.6) was written in user-defined function (UDF) to calculate the rotation speed.

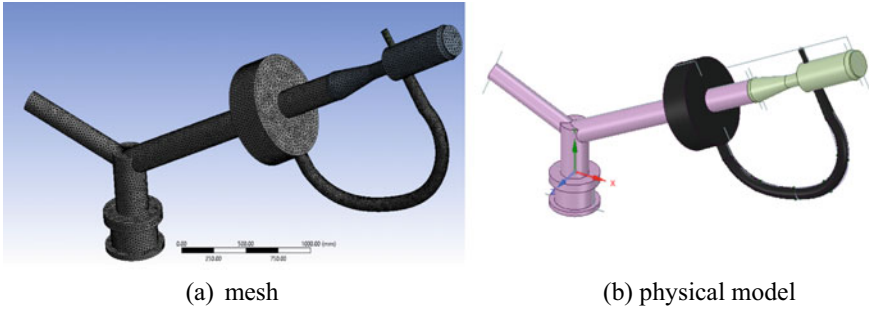
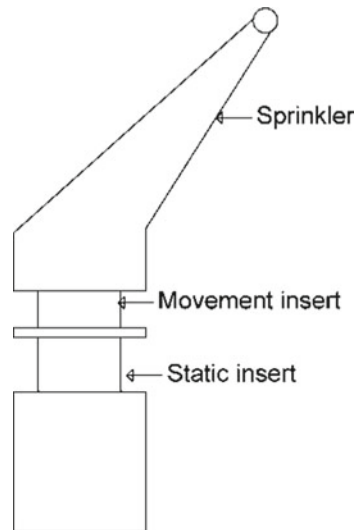


Fig. 3.3 3D model and unstructured mesh

Fig. 3.4 Schematic diagram of static and movement insert of the sprinkler



3.2.3.1 Mathematical Model

The momentum equation, shown below, is dependent on the volume fractions of all phases through the properties ρ and μ .

$$\frac{\partial}{\partial t}(\rho \vec{v}) + \nabla \cdot (\rho \vec{v} \vec{v}) = -\nabla \rho + \nabla \cdot [\mu(\nabla \vec{v} + \nabla \vec{v}^T)] + \rho \vec{g} + \vec{F} \quad (3.1)$$

The energy equation as shown in the equation below.

$$\frac{\partial}{\partial t}(\rho E) + \nabla \cdot (\vec{v}(\rho E + \rho)) = \nabla \cdot (k_{eff} \nabla T) + S_h \quad (3.2)$$

where $E =$ VOF model treats energy, $T =$ temperature as mass-averaged variables and can be expressed as Eq. (3.3)

$$E = \frac{\sum_{q=1}^n a_q P_q}{\sum_{\rho=1}^n a_q P_q E_q} \quad (3.3)$$

where E_q for each phase is based on the specific heat of that phase and the shared temperature.

The properties ρ and k_{eff} (effective thermal conductivity) are shared by the phases. The source term S_h contains contributions from radiation, as well as any other volumetric heat sources.

The FLUENT models selected are standard $k-\varepsilon$, RNG $k-\varepsilon$, realizable $k-\varepsilon$ and so on. The working principle of the fluidic sprinkler is based on gap-liquid flow. The Governing equations for unsteady, three dimensional and viscous flow is given as:

$$\begin{aligned} \partial(\overline{\rho u_i \varepsilon}) / \partial \chi_j &= \frac{\partial}{\partial \chi_j} + \left(a_\kappa \mu_{eff} \frac{\partial}{\partial \chi_j} \right) + \mu_i s^2 - \rho \varepsilon \\ \mu_{eff} &= \mu + \mu_i s = \sqrt[3]{2} S_{ij} S_{ij} \end{aligned} \quad (3.4)$$

where $\mu_{eff} =$ effective viscosity, $\alpha_\kappa =$ Prandtl number in k equation pulsation rate equation (ε equation) in the model, $R =$ source item created by deformation rate

$$\partial \left(\frac{\rho u_i \varepsilon}{\partial \chi_i} \right) = \frac{\partial}{\partial \chi_i} \left(a_\varepsilon \mu_{eff} \frac{\partial \varepsilon}{\partial \chi_i} \right) + c_{i\varepsilon} \mu_i S^2 \frac{\varepsilon}{\kappa} - C_{2\varepsilon} \rho \frac{\varepsilon^2}{\kappa} - R \quad (3.5)$$

3.2.3.2 Rotation Speed

The rotation speed of the sprinkler can be written as specified equation below.

$$\begin{aligned} KE_R &= \frac{1}{2} I w^2 Q, \quad w = \frac{d\theta}{dt}, \\ KE_R &= \frac{1}{2} I \left(\frac{d\theta}{dt} \right)^2 Q \\ \frac{2KE_R}{IQ} &= \left(\frac{d\theta}{dt} \right)^2 \\ \sqrt{\frac{2KE_R}{IQ}} &= \frac{d\theta}{dt} \end{aligned}$$

$$dt = \frac{d\theta}{\sqrt{\frac{2KE_R}{IQ}}} \tag{3.6}$$

where I = moment of initial; KE_R = rotational kinetic energy; $d\theta$ = angular displacement; dt = time; M = mass of the sprinkler

Coefficient (Q) is given as

$$Q = \frac{3}{4} \left(\frac{Cd}{r} \right) \left(\frac{\rho a}{\rho w} \right) \tag{3.7}$$

where Cd = the frictional resistance and is assumed to be 0.44; ρa = Air density (1.29 kg m^3); r = radius of the sprinkler r nozzle (7.5 mm), ρw = Water density ($1 \times 103 \text{ kg m}^3$). Therefore when dt is known, the rotation speed can be calculated.

3.2.3.3 Grid Sensitivity Analysis

The grid generation is the next step required to perform after geometry creation. It is one of the tedious and time-consuming parts. To solve the Navier- Stokes equation numerically, the commercial code ANYS 19.2 workbench was adopted to conduct the numerical calculation. The full flow fields were divided into different fluid domains and each of them was meshed by unstructured hexahedron mesh via the CFD. An independence test was performed to ensure the independence of a solution with mesh size as shown in Fig. 3.5. The variation in velocity was found to be negligible after 1.35 million lakh elements compared to the other grid elements, hence the grid size of 1.35 million lakh was chosen to conduct the simulation.

Fig. 3.5. Grid independence check

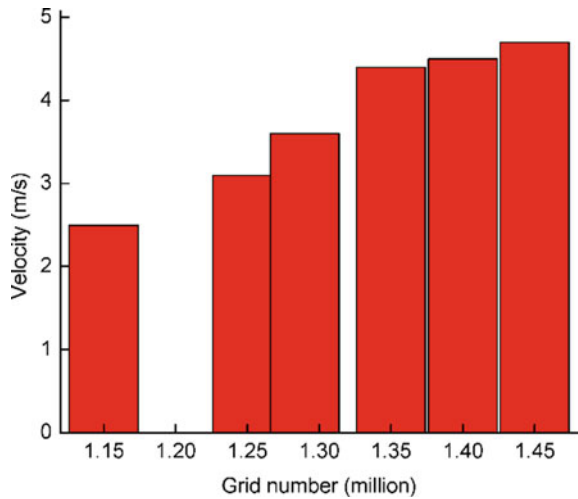


Table 3.1 Boundary conditions of the sprinkler

Rotation angle (°)	Pressure (kPa)	Nozzle size (mm)	Length of a tube (mm)
90	100	3	15
180	150	4	20
270	200	5	25
360	250	6	30
	300	7	

3.2.3.4 Boundary Conditions

Generally, boundary conditions are needed to be specified on all surfaces of the computation domain. The inlet condition was as pressure, and the outlet condition was set by the outflow. All physical surfaces of the sprinkler were set as non-slip walls. Standard walls functions were used at the solid wall, air and water were used as the working fluid. The convergences precession of the calculation was set at 0.0001. Table 3.1 presents the parameters used in the numerical simulation and experiment. The reason for using these parameters was to compare the performance of each parameter and select the best combination for the sprinkler.

3.2.3.5 Experimental Procedure

The materials used for the experiment include; centrifugal pump, electromagnetic flow meter, and piezometer, valve and dynamic fluidic sprinkler. The sprinkler was installed at a height of 2 m from the ground level with nozzle an elevation angle of 23°. The riser was at an angle of 90° to the horizontal from which was 0.9 m above the ground. Water was pumped from the reservoir through the main pipe and sprayed out from the nozzle as shown in Fig. 3.6. The working pressure was measured by a pressure gauge at the base of the sprinkler had an accuracy of 0.4%. To standardize the laboratory conditions, the sprinkler was run for 20 min before performing the actual experiments. The experiment aimed to determine quadrant completion times for each nozzle and droplet size. Both nozzle and working pressures were all within the manufacturer's recommendations and were varied from 100 ~ 300 kPa. To determine the rotation uniformity from one quadrant to another, the total area of rotation was divided into four quadrants and each experiment lasted for 1 h. Quadrants Q1, Q2, Q3 and Q4 comprised of radial lines 0, 90; 90, 180; 180, 270 and 270, 0, respectively.

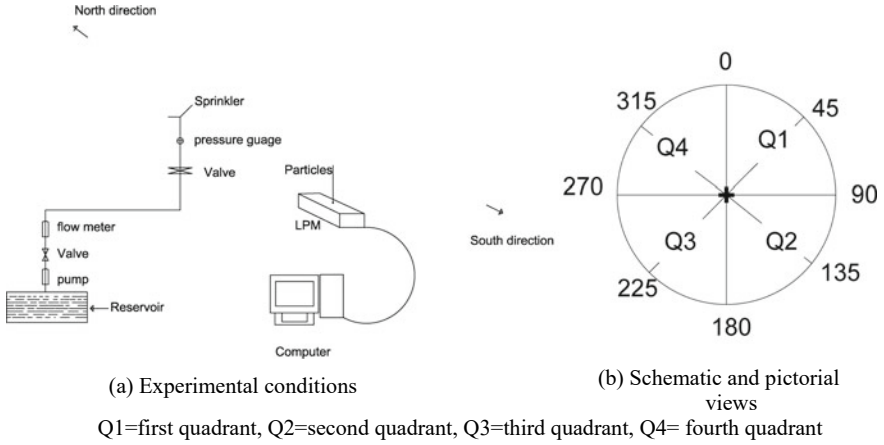


Fig. 3.6 The layout of cans around the sprinkler in the indoor laboratory

To investigate the sprinkler rotation speed uniformity, a stopwatch was used to record the time taken by the sprinkler to move from one quadrant to the other, in the course of the one-hour duration. Three replications of completion time through the quadrants were recorded for each sprinkler-nozzle-pressure configuration. Drop sizes were measured using a Thies Clima Laser Precipitation Monitor (LPM) was from Adolf Thies GmbH and Co. KG, Gottingen, Germany. Measurements were conducted indoors with no wind at a pressure of 100, 150, 200, 250 and 300 kPa. The LPM measures drop sizes from 0.125 mm to 6.0 mm. Drop size measurements were grouped into 0.1 mm increments (± 0.05 mm) for analysis starting with 0.25 mm continuing to 5.95 mm. Measured drops less than 0.2 mm in diameter were discarded as they represent less than 0.01% of the total volume of drops measured. The sprinkler nozzle was located 2 m above the laser beam of the LPM. Measurements were collected at the middle (6 m) and end (12 m) positions of radial distances from the sprinkler. Droplet size parameters used in this study include D_v = average volume diameter and (d, mm) = arithmetic mean diameter as shown in Eqs. (3.8) and (3.9)

$$\bar{d} = \frac{\sum_{i=1}^n m_i d_i}{\sum_{i=1}^n m_i} \tag{3.8}$$

$$d_v = \frac{\sum_{i=1}^n m_i d_i^4}{\sum_{i=1}^n m_i d_i^3} \tag{3.9}$$

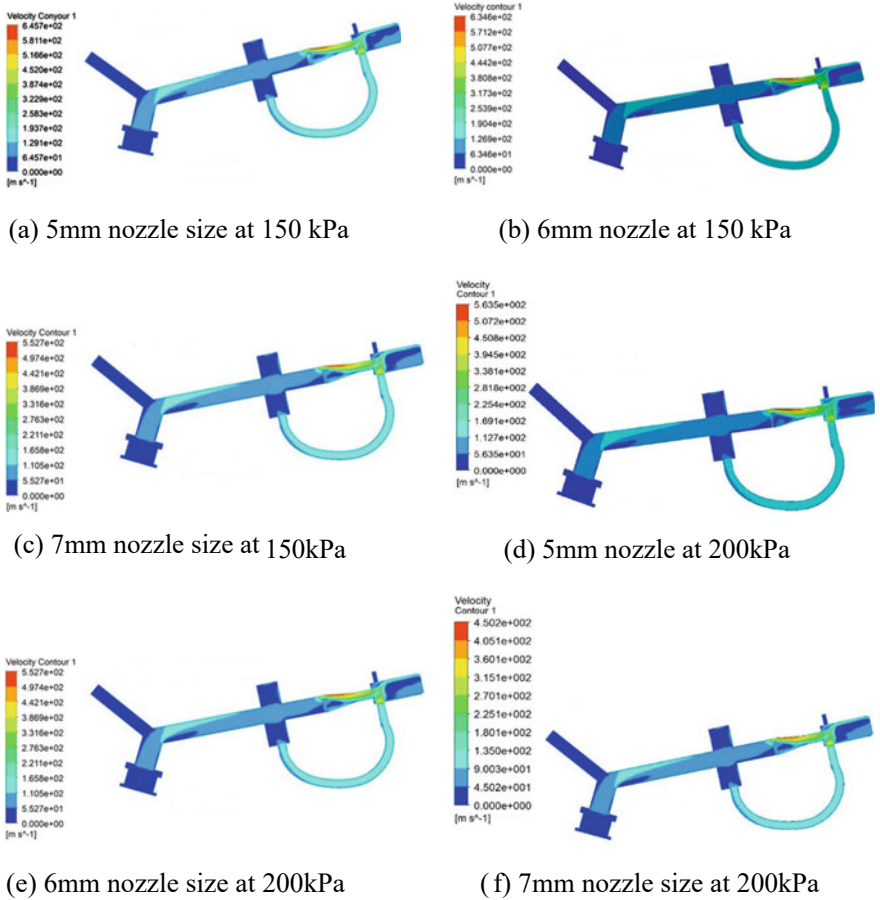


Fig. 3.7 Relationship between velocity and nozzle sizes

3.3 Results and Discussion

3.3.1 Relationship Between Velocity Distribution and Nozzle Sizes

Numerical simulations were carried out to identify velocity distribution within the dynamic fluidic sprinkler with different types of nozzle sizes under a pressure of 150 and 200 kPa. For both pressures velocity distribution decreased steadily as the nozzle sizes increased. Generally, low-velocity gradients existed in 7 mm nozzle size, which improved when the pressure was increased.

There was some flow distortion observed very close to the fluidic element for all the nozzle sizes. This however improved as the nozzle size was increased. The

maximum velocity occurred around the fluidic element. This phenomenon is caused by a reduction in pressure on the inner side of the jet due to the entrainment of fluid by the jet. This supports already established results from earlier research works. The 5 mm nozzle size, however, had relatively higher velocity distribution along the surface with a 7 mm nozzle having lower distribution. At the pressure of 200 kPa, the trend was the same. The 5 mm nozzle size saw much improvement in velocity distribution with a low-pressure region. This means that a 5 mm nozzle size could be ideal for field application to maximize the range under the given pressure while avoiding the cost of crop production in sprinkler irrigated fields (Fig. 3.7).

3.3.2 Relationship Between Velocity and Length of the Tube

The relationship between the velocity distribution, length of the tube, and nozzle diameter of 5 mm under different working pressure is shown in Fig. 3.8.

There was some distortion observed close to the inlet of tube length especially 15 mm. Distortion reduced as the length of the tube was increased. Velocity distribution within the tube was much better especially with the 25 mm length of the tube. It was found that the distortion on the 25 mm length of the tube is smaller compared with the other length of the tube. This means that by using a 25 mm tube length, the test sprinkler can achieve better rotation speed. The 15 mm length had a relatively lower velocity distribution along the surface. As pressure was increased velocity also increased, meanwhile velocity distribution was not improved compared with 150 kPa. A possible reason could be that more pressure is been built within the tube resulting in low velocity. It can, therefore, be concluded that the test sprinkler with 5 mm nozzle size, 25 mm tube length, and 150 kPa combination will work efficiently from a water distribution perspective.

3.3.3 Comparison of the Numerical Simulation, Calculated and Experimental Results

An empirical equation for the variation trend of the rotation speed of different nozzles, length of the tube and operating pressures were generated by using curve fitting. The proposed equation is sufficiently accurate and simple to use for rotation speed. According to the equation, the nozzle diameter, length of the tube and the working pressure had a significant influence on the rotation speed of the test sprinkler. Comparing the fitted values, simulated and experimental data, the relative error (*er*) was less than 4% which means the analysis of the relationship between rotation speed and nozzle diameters, length of tube and pressure is accurate.

$$Sp = 11.5D_2^{0.001}L^{-0.99}P^{0.1} \quad (3.10)$$

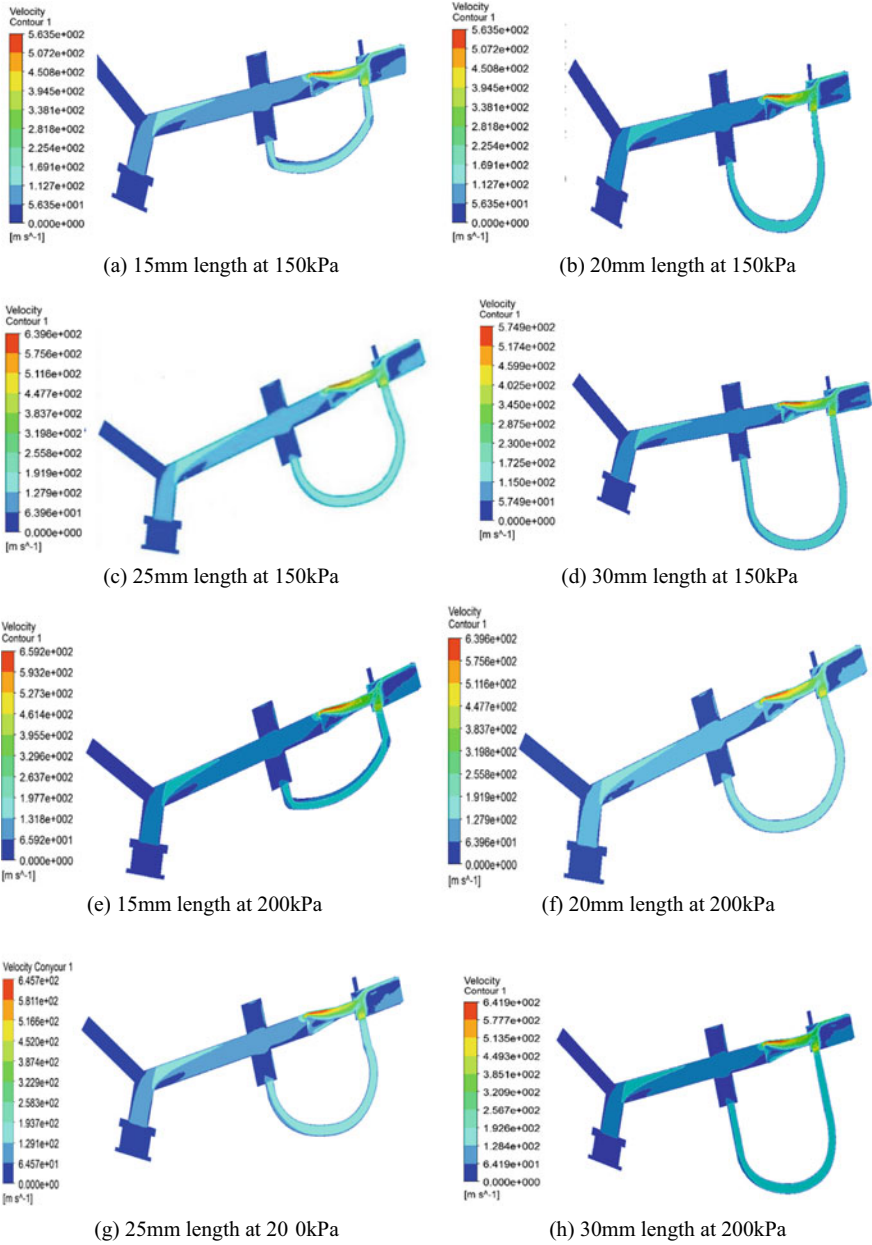
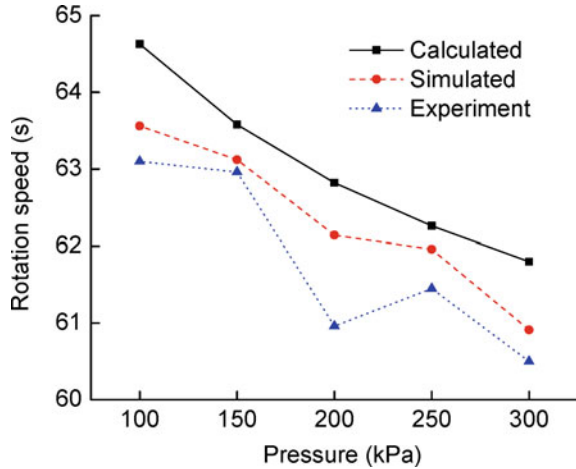


Fig. 3.8 Relationship between velocity and length of the tube

Fig. 3.9 Comparison of the numerical simulation and experimental results



where Sp is the rotation speed (seconds), $D2$ is the nozzle diameter (mm), L length of the tube (mm) and p is the working pressure (kPa).

Computational results from numerical simulations and experiments were matched with the calculated shown in Fig. 3.9 and Table 3.2. From the simulated results, 5 mm nozzle size and 25 mm tube length were found to be ideal. Hence, 5 mm nozzle size and 25 mm tube length were selected for further testing.

From the study, it can be seen that simulated, calculated and experimental dropped gradually as the pressure was increased, and the trend between the calculated and simulated was quite similar. The experimental results were; however, lower than simulated and calculated results. The relative errors at 150 kPa were 0.73, 0.90 and 0.25 simulated, calculated and experiment, respectively. The computational results were relatively higher than experimental results and comparatively lower than the calculated results. This could be attributed to the fluctuation of pressure and external factors. The minimum average deviation between the calculated, simulation and experiment was 0.25%, while the maximum was 0.90%. Notwithstanding, the deviations were minimal and therefore the numerical results agreed well with the experimental results and this affirmed the reliability of the empirical equation been generated.

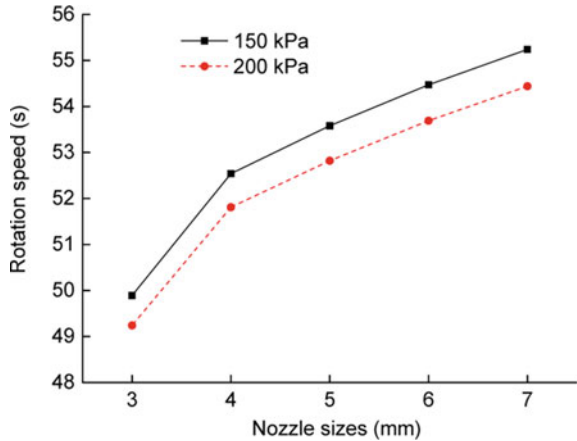
3.3.4 Comparison of Rotation Speed and the Nozzle Sizes

Rotation time measures the period of sprinkler rotation. This can be performed by recording the rotation speed of the sprinkler by using a stopwatch. A fast rotation rate causes a stream jet to bend and creates gaps in the pattern due to friction. However, the slow rate increases application intensity so long as the jet stream remains situational. The repetition of spray intensity floods soil surface and instantaneously prevents air

Table 3.2 Comparison of the numerical simulation, calculated and experimental results for 5.5 mm nozzle size

Pressure (kPa)	Simulated (s)	Calculated (s)	Relative error	Calculated (s)	Experiment (s)	Relative error	Simulated (s)	Experiment (s)	Relative error
100	63.56	64.63	1.68	64.63	63.1	2.42	63.56	63.1	0.73
150	63.12	63.58	0.73	63.58	62.96	0.98	63.12	62.96	0.25
200	62.14	62.82	1.09	62.82	60.96	3.05	62.14	60.96	1.94
250	61.96	62.26	0.49	62.26	61.45	1.32	61.96	61.45	1.48
300	60.91	61.8	0.02	61.8	60.5	2.14	60.91	60.5	0.68

Fig. 3.10 Comparison of rotation speed and nozzle sizes



escape from soil media resulting in surface run-off and sheet erosion. Figure 3.10 shows the relationship between the rotation speed and the nozzle sizes at 150 and 200 kPa.

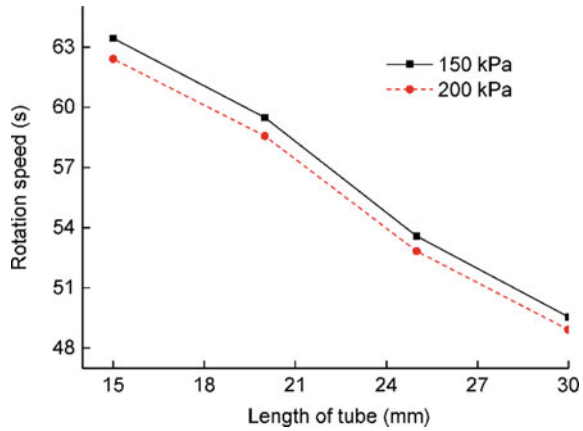
From the study, it was revealed that the rotation speed increases approximately linearly as the nozzle size increases. As the pressure increases the rotation speed decreases for all the nozzles size. It was found that rotation speed was, however, smaller with smaller nozzle diameters and this is because smaller diameters have greater velocities which make the sprinkler rotate faster. It also appears that when the nozzle was smaller than 5 mm, the rotation speed reduced below 55 s, which means that sprinklers might not operate efficiently. When the nozzle size was too large, the sprinkler tends to give higher rotation speed. This is because less pressure is been built within the sprinkler resulting in low rotation speed. Variations in rotation speed were 14.5, 13.8, 14.1 s, and 14.9 s for 3, 4, 5, 6, and 7 mm, respectively. A comparison of nozzle sizes demonstrated that 5 mm nozzle size gave optimum rotation stability compared with other types of nozzles used in this study. These results are slightly better than those obtained by.

3.3.5 Relationship Between Rotation Speed and Length of the Tube

Figure 3.11 shows the relationship between the rotation speed and the length of the tube at 150 and 200 kPa. In this study, a 5 mm nozzle was maintained whiles the pressure and length of the tube were varied. From the graph, it can be seen that as the length of the tube increases rotation speed also decreases. This could be attributed to a loss of pressure in the length of the tube resulting in low rotation speed.

Comparatively, 200 kPa decreased slightly as the length of the tube increased. With an increase in tube length, 25 mm appears to produce optimum results compared with

Fig. 3.11 Relationship between rotation speed and length of the tube



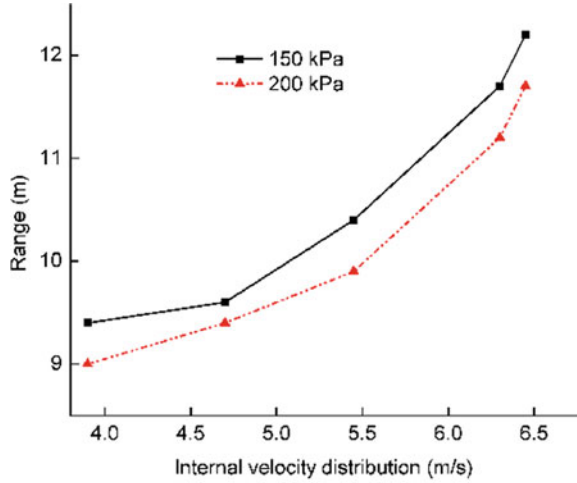
the other length of tubes. It was found that the differences in rotation speed were insignificant ($p > 0.05$). From the graph, it can be observed that the length of the tube had a slight influence on the rotation speed of the test sprinkler.

3.3.6 *Effect of Internal Velocity Distribution on Hydraulic Performance*

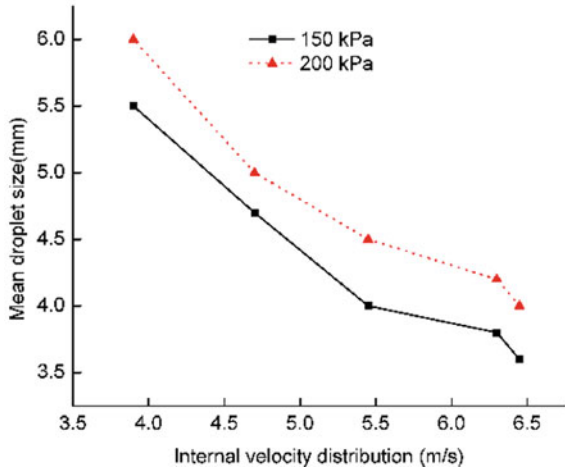
The shape of the water distribution pattern, uniformity, range, droplet size, and velocities is mainly determined by the sprinkler model and its internal design, discharge angle and jet breakup mechanism. The relationship between internal velocity distribution, a distance of throw and droplet size with different nozzles diameter under a different working pressure of 150 and 200 kPa is shown in Fig. 3.12. The distance of throw increased with an increase in pressure. This is possible because, at a high-velocity condition, the jet breaks up quickly, resulting in a higher radius of throw.

It can be observed from the figure that the velocity distribution increased as the size of the droplets decreased for both pressures. For both pressures, optimum velocity was obtained at 5 m-s and thereafter decreased as the velocity increases, which can maximum losses caused by wind drift and evaporation. These results are similar to those obtained by previous researchers who used different sprinkler types. Using a 5 mm nozzle size will produce optimum droplet sizes, which can fight wind drift and evaporation losses. This is because large droplets possess high kinetic energy, and on impact, they disrupt the soil surface, especially soils with crustiness problems, leading to sealing of the soil surface.

Fig. 3.12 Relationship between velocity, range and droplet size



(a) Range



(b) Mean droplet size

References

1. Clemmens AJ, Dedrick AR (1994) Irrigation techniques and evaluations. *Adv Ser Agric Sci* 14:64–103
2. Hendawi M, Molle B, Folton C, Granier J (2005) Measurement accuracy analysis of sprinkler irrigation rainfall in relation to collector shape. *J Irrig Drain Eng* 131:477–483
3. Sourell H, Faci JM, Playan E (2003) Performance of rotating spray plate sprinklers indoor experiments. *J Irrig Drain Eng* 129:376–380
4. Li J, Kawano H (1995) Simulating water-drop movement from noncircular sprinkler nozzles. *J Irrig Drain Eng* 121(6):152–158

5. Yan HJ, Jin HZ (2004) Study on the discharge coefficient of non-rotatable sprays for center-pivot system. *J Irrig Drain* 23:55–58
6. Yan HJ, Liu ZQ, Wang FX, Yang XG, Wang M (2007) Research and development of impact sprinkler in China. *J China Agric Univ* 12:77–80
7. Yuan SQ, Zhu XY, Li H, Ren ZY (2005) Numerical simulation of inner flow for complete fluidic sprinkler using computational fluid dynamics. *Trans CSAM* 36(10):46–49
8. Yan HJ, Ou YJ, Kazuhiro Xu CB (2009) Numerical and experimental investigations on internal flow characteristic in the impact sprinkler. *Irrig Drain Syst* 23:11–23
9. Palfrey JR, Liburdy JA (1986) Mean flow characteristic of turbulent offset jet. *Trans ASME* 108:82–88
10. Bourque L, Newman BG (1960) Reattachment of two-dimension incompressible jet to an Adjacent flatplate. *Aeronaut Q* 11:201232. <https://doi.org/10.1017/S000192590001797>
11. Hoch J, Jiji LM (1981) Two dimensions turbulent offset jet-boundary interaction. *Trans ASME* 103:154–161
12. Song HB, Yoon SH, Lee DH (2000) Flow and heat transfer characteristic of a two-dimensional oblique wall attaching offset jet. *Int J Heat Mass Transf* 43:2395–2404
13. Wang Q, Lu Y (1996) Theoretical laws for determining the main parameters of a wall-attachment jet flow. *J Jilin Agric Univ* 18:69–71
14. Liu JP, Yuan SQ, Li H, Zhu XY (2013) Numerical simulation and experimental study on a new type variable-rate fluidic sprinkler. *J Agric Sci Technol* 15(3):569–581
15. Zhu X, Yuan S, Liu J (2012) Effect of sprinkler head geometrical parameters on the hydraulic performance of fluidic sprinkler. *J Irrig Drain Eng* 138(11):1943–4774
16. Dwomoh FA, Shouqi Y, Hong L (2014) Sprinkler rotation and water application rate for the newly designed complete fluidic sprinkler and impact sprinkler. *Int J Agric Biol Eng* 7(4):38–46. <http://doi10.9790/1684-11467073>
17. Hu G, Zhu XY, Yuan SQ, Zhang LG, Li YF (2019) Comparison of ranges of fluidic sprinkler predicted with BP and RBF neural network models. *J Drain Irrig Mach Eng.* 37(3):263–269
18. Li H, Yuan SQ, Liu JP, Xiang QJ, Zhu XY, Xie FQ (2007) Wall-attachment fluidic sprinkler. Ch. Patent No. 101224444 B
19. Liu JP, Liu XF, Zhu XY, Yuan SQ (2016) Droplet characterization of a complete fluidic sprinkler with different nozzle dimensions. *Biosyst Eng* 65(4):2–529
20. Zhu XY, Fordjour A, Yuan SQ, Dwomoh F, Ye DX (2018) Evaluation of hydraulic performance characteristics of a newly designed dynamic fluidic sprinkler. *Water* 10, 1301. <https://doi.org/10.3390/w10101301>
21. Han S, Evans RG, Kroeger MW (1994) Sprinkler distribution patterns in windy conditions. *Trans ASAE* 37(5):1481–1489